Available online at www.sciencedirect.com
SCIENCE DIRECT
Journal of Solid State Chemistry 179 (2006) 2190–2198
JOURNAL OF SOLID STATE CHEMISTRY
www.elsevier.com/locate/jssc

As–As dimerization, Fermi surfaces and the anomalous electrical transport properties of UAsSe and ThAsSe

Ray L. Withers[a,*], Herman J.P. van Midden[b], Albert Prodan[b], P.A. Midgley[c], J. Schoenes[e], R. Vincent[d]

[a]*Research School of Chemistry, Australian National University, Canberra, ACT 0200, Australia*
[b]*Jozef Stefan Institute, Jamova 39, SI-1000 Ljubljana, Slovenia*
[c]*Department of Materials Science and Metallurgy, University of Cambridge, Pembroke Street, Cambridge CB2 3QZ, UK*
[d]*H.H.Wills Physics Laboratory, University of Bristol, Bristol, BS8 1TL, UK*
[e]*Institut für Physik der Kondensierten Materie, Technical University Braunschweig, D-38106 Braunschweig, Germany*

Received 14 February 2006; received in revised form 4 April 2006; accepted 9 April 2006
Available online 25 April 2006

Abstract

A temperature dependent electron diffraction study has been carried out on UAsSe to search for evidence of As–As dimerization at low temperature. A highly structured characteristic diffuse intensity distribution, closely related to that recently reported for ThAsSe, has been observed at low temperature and interpreted in terms of a gradual charge density wave type phase transition upon lowering of temperature involving disordered As–As dimerization within (001) planes. Plausible models of the proposed As–As dimerization have been obtained using a group theoretical approach. Electronic band structure calculations of ThAsSe and UAsSe have been used to search for potential Fermi surface nesting wave-vectors. The results are in good agreement with the experimentally observed diffuse intensity distributions in both cases.

Keywords: Kondo effect; As–As dimerization; Electron diffraction; Incommensurately modulated; Fermi surface nesting; Band structure

1. Introduction

Ever since the initial growth of UAsSe and ThAsSe single crystals [1] and the first measurements of their electrical transport properties [2,3], the anomalous temperature dependence of their basal plane electrical resistivity (see Fig. 1) has fascinated researchers and led to controversial and ever-changing interpretations [2–18]. In the case of UAsSe, Wojakowski et al. [2] found a characteristic logarithmic decrease of the electrical resistivity with increasing temperature up to ~50 K and again immediately above the ferromagnetic onset temperature of T_C~109 K all the way up to 700 K. The latter behaviour initially suggested a scattering mechanism of magnetic origin related to the original Kondo effect [4]. Early investigations thus concentrated on the determination of the low temperature ferromagnetic structure and its relation to the electronic structure [5–8].

In 1988, however, Schoenes et al. [3] pointed out that since the isostructural but apparently diamagnetic compound ThAsSe also displays a rather similar logarithmic decrease of the basal plane resistivity from ~70 K up to ~500 K, a straightforward interpretation in terms of a magnetic Kondo effect had to be ruled out. In 1995, Henkie et al. [9] fitted resistivity data for UAsSe with the Kondo formula and claimed that the anomalous part of the resistivity could be described in terms of single impurity behaviour in the Kondo limit of the Anderson model. It was furthermore claimed that this non-magnetic Kondo like scattering was "…most probably induced by (As/Se substitutional) anion disorder…" [9]. Later Cox and Zawadowski [10] and Henkie et al. [11] proposed a positionally disordered two level system Kondo model, the latter again suggesting that the assumed two-state local positional disorder was induced by (As/Se) anion disorder.

*Corresponding author. Fax: +61 2 6125 0750.
E-mail address: withers@rsc.anu.edu.au (R.L. Withers).

0022-4596/$ - see front matter © 2006 Elsevier Inc. All rights reserved.
doi:10.1016/j.jssc.2006.04.016

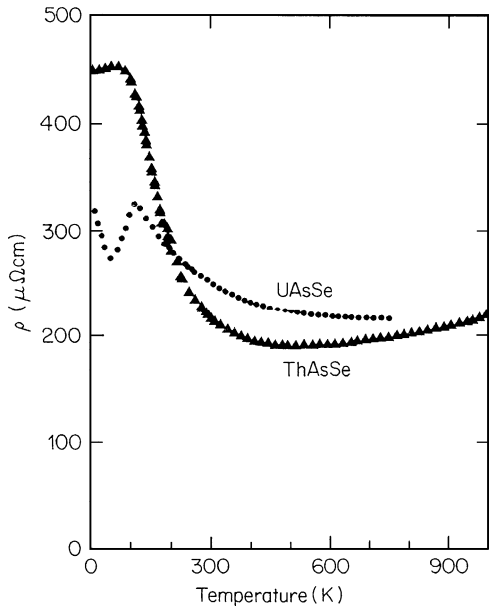

Fig. 1. The temperature-dependent basal plane electrical resistivity of UAsSe and ThAsSe.

The effect of As/Se disorder has subsequently been pursued further [12–18]. It is found that the basal plane resistivity in the paramagnetic state of UAsSe ($>\sim$110 K) is virtually sample independent. It is apparently only in the very lowest temperature ferromagnetic state below $\sim$50 K that As/Se disorder affects the resistivity.

Various alternative scenarios to explain the observed resistivity behaviour, like an order–disorder transformation, charge disproportionation, electron charge localization as well as charge density wave (CDW) formation associated with As–As dimerization, were discussed by Schoenes et al. [3]. The latter was considered most likely on crystal chemical grounds, particularly since dimerization of the anions in the As position is a common feature of compounds crystallizing in the underlying *ZrSiS* average structure type (see e.g. [19]).

Recently, the first direct evidence for As–As dimerization was reported in the case of ThAsSe [20]. The evidence took the form of a highly structured, planar diffuse intensity distribution apparent in low temperature electron diffraction patterns (EDPs). It was interpreted in terms of the occurrence of a gradual CDW type phase transition involving localization of electrons associated with As ions via As–As dimerization (or covalent bonding) upon lowering of temperature. While dimerization of the anions in the As positions is common for compounds crystallizing in the underlying *ZrSiS* average structure type, the pattern of such dimerization is usually rather simple as e.g. in the case of $(La^{3+})_2(Se_2)^{2-}(Se^{2-})_2$, where the $(Se_2)^{2-}$ dimers (in the equivalent layers to that of the As ions in ThAsSe) pack in a relatively simple, commensurate herringbone type array—see e.g. Fig. 2 of [20].

In the case of ThAsSe, however, the observed diffuse distribution implied disordered As–As dimerization (of some but not all As ions) along $\langle 110 \rangle$ directions within (001) planes with an effectively incommensurate real space periodicity [20]. This casts some doubt on the originally proposed low temperature $(Th^{4+})_2(As_2)^{4-}(Se^{2-})_2$ picture [3] in which one might expect a relatively simple, commensurate herringbone type packing of $(As_2)^{4-}$ dimers. The underlying reason for the effectively incommensurate, although close to seven times, real space periodicity along the $\langle 110 \rangle$ directions is not at all apparent [20]. Nor are the implications as regards the local oxidation states of the Th, As and Se ions in ThAsSe or the mechanism for basal plane conductivity. Nonetheless, if such As–As dimerization is observed for ThAsSe, then it ought also to be observed for UAsSe.

The first purpose of the current paper therefore is to present the results of a low temperature electron diffraction study of UAsSe again looking for direct evidence of As–As dimerization. The second purpose of the paper is to present the results of electronic band structure calculations of ThAsSe and UAsSe in an effort to understand the origin of the real space periodicities of As–As dimerization along the $\langle 110 \rangle$ directions implied by the observed diffuse distributions. Extended Hückel tight binding calculations of the Fermi surfaces (FSs) of ThAsSe and UAsSe are used to predict possible nesting wave-vectors for comparison with the experimentally observed structured diffuse intensity distributions in both cases.

2. Experimental

2.1. Synthesis

The as-grown single crystal specimens of nominal stoichiometry UAsSe and ThAsSe investigated in this study were grown by Dr. F. Hulliger at ETH, Zürich. The synthesis procedure is described in [1]. The crystals took the form of thin plates perpendicular to the **c** axis of the ZrSiS average structure type shown in Fig. 2. Specimens suitable for observation in the Transmission Electron Microscope (TEM) were obtained by crushing. The specimens were examined in a Philips EM 430 TEM operating at 300 kV. A liquid N_2 cooling holder was used for the low temperature work on the UAsSe specimen.

2.2. Electron diffraction

Fig. 3a shows a typical [001] zone axis electron diffraction pattern (EDP) of UAsSe taken at 90 K. For comparison purposes, Fig. 3b shows the equivalent [001] zone axis EDP of ThAsSe taken at 100 K (see [20]). At room temperature, in the case of UAsSe, no equivalent diffuse distribution to that shown in Fig. 3a could be detected at all. In the case of ThAsSe, however, a remarkably similar but weaker diffuse distribution was still apparent even at room temperature (see Fig. 3c). Note that the amplitude of the diffuse streaking in the case of

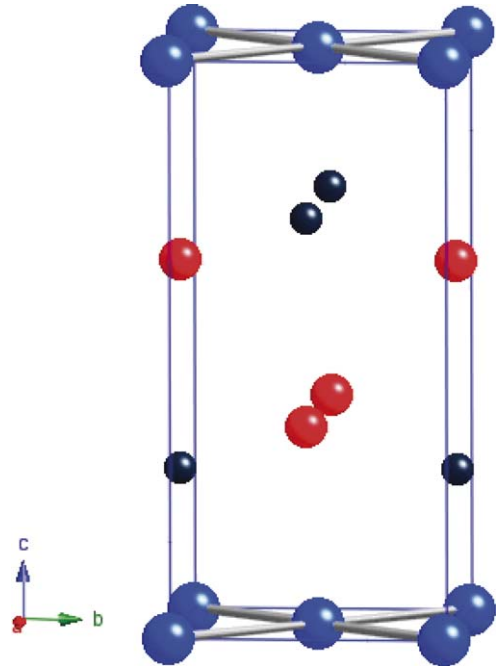

Fig. 2. The *P*4/*nmm* (Origin Choice 2), ZrSiS type average structure of ThAsSe projected close to [100]. The As atoms are represented by the large (blue) balls, the Th ions by the small (black) balls and the Se ions by the medium sized (red) balls. The covalent bonding between the As atoms is represented by the grey rods.

UAsSe is significantly weaker than in the case of ThAsSe making it rather more difficult to successfully record.

In addition to the strong Bragg reflections of the underlying, *P*4/*nmm* average structure (see Fig. 3), note the presence in both UAsSe and ThAsSe of a clearly closely related, diffuse intensity distribution in the form of orthogonal $\mathbf{G} \pm \chi[110]^* \pm \varepsilon[1\bar{1}0]^*$ and $\mathbf{G} \pm \chi[1\bar{1}0]^* \pm \varepsilon[110]^*$ (χ fixed, ε continuous in both cases) 'lines' of diffuse streaking running along the $[1\bar{1}0]^*$ and $[110]^*$ directions of reciprocal space, respectively, around the nominally *n* glide forbidden $hk0$, $h+k$ odd reflections. (The family of Bravais lattice allowed Bragg reflections of the parent structure are labelled as **G** here, including the nominally *n* glide forbidden $hk0$, $h+k$ odd, reflections.) In the case of UAsSe, χ as measured from Fig. 3a $= 0.125(10)$ while, in the case of ThAsSe, $\chi = 0.140(10)$ as measured from Fig. 3b and does not vary noticeably with temperature (cf. e.g. Fig. 3b with 3c). The method used to measure the fixed parameter χ characteristic of the diffuse streaking directly from the EDP's is shown in Fig. 3a and b. Note that the well-defined magnitude of χ makes it effectively a one-dimensional primary modulation wave-vector **q** whose inverse defines a corresponding real space modulation periodicity along the $\langle 110 \rangle$ directions of real space, given by $1/\chi$ i.e. ~ 8 $\langle 110 \rangle$ for UAsSe and ~ 7 $\langle 110 \rangle$ for ThAsSe.

As was also the case for ThAsSe [20], note the characteristic extinction condition that the $\mathbf{G} \pm \chi\langle 110 \rangle * \pm \varepsilon\langle 1\bar{1}0 \rangle *$ diffuse streaking in Fig. 3a occurs only around

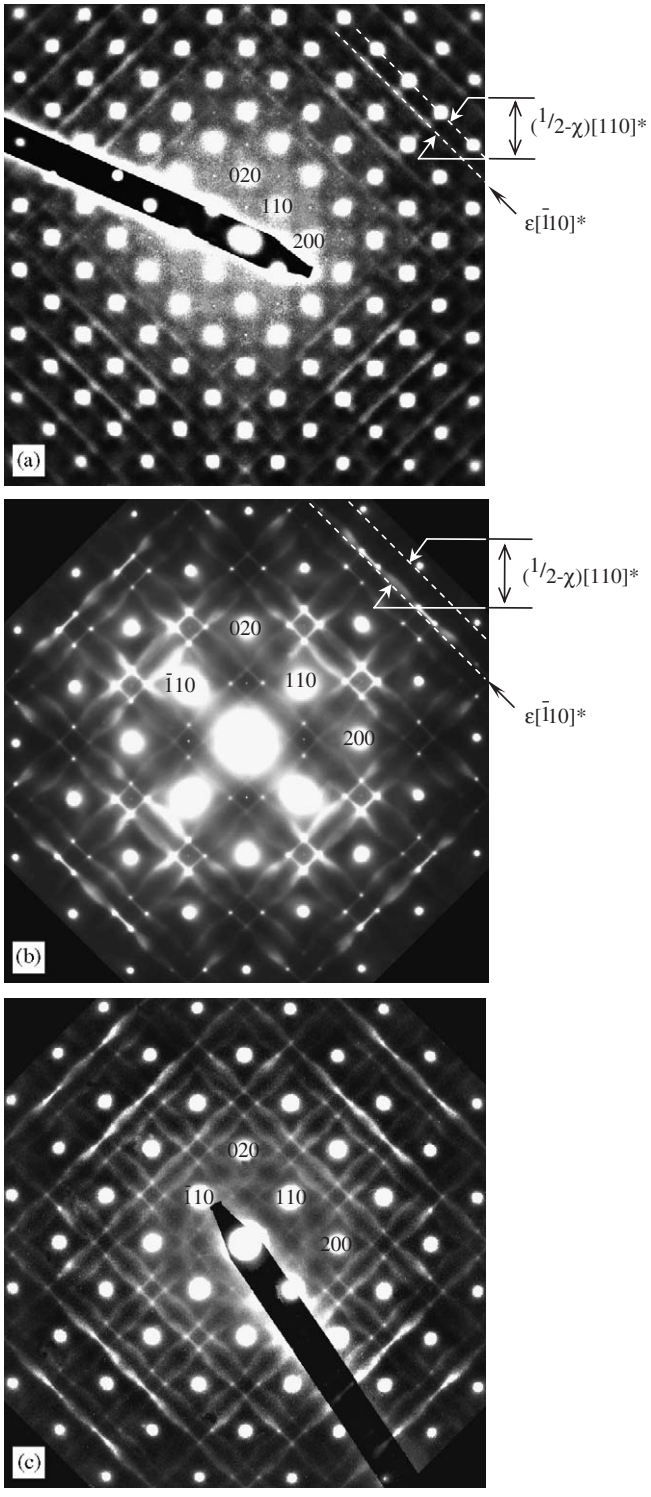

Fig. 3. (a) A typical $\langle 001 \rangle$ zone axis EDP of UAsSe taken at ~80–90 K, (b) ThAsSe taken at 100 K and (c) ThAsSe at room temperature. In addition to the strong Bragg reflections of the underlying *P*4/*nmm* average structure, note the presence of a highly structured characteristic diffuse intensity distribution in the form of two orthogonal 'lines' of diffuse streaking running along the $\mathbf{G} \pm \chi\langle 1\bar{1}0 \rangle^* + \varepsilon\langle 110 \rangle^*$ ($\chi \sim 0.125$ in the case of UAsSe and ~0.14 in the case of ThAsSe and ε continuous) positions of reciprocal space around the nominally *n* glide forbidden *hk*0, $h+k$ odd reflections. The method used to measure the fixed parameter χ characteristic of the diffuse streaking directly from the EDPs is shown in Figs. 3a and b.

the $\mathbf{G} = [hk0]^*$, $h+k$ odd, but not even, reflections. The existence of just such a characteristic extinction condition strongly suggests that As–As dimerization along $\langle 110 \rangle$ is primarily responsible (see [20,21] and below). Again, as also occurs in the case of ThAsSe, the diffuse 'lines' are clearly strongly transverse polarized [21] e.g. the $\mathbf{G} \pm 0.125[110]* \pm \varepsilon[1\bar{1}0]*$ diffuse 'lines' in Fig. 3a are most intense when looking out along the [110]* direction of reciprocal space and absent along the orthogonal $[1\bar{1}0]^*$ direction, etc. The corresponding As atomic displacements must then also run, or be polarized, along [110]. Likewise, a strongish 'size effect' is again apparent in that the intensity distribution of the $\mathbf{G} \pm 0.125\langle 110\rangle^* \pm \varepsilon\langle 1\bar{1}0\rangle^*$ lines is strongly asymmetric [20], with the lines on the high angle side of the particular $\mathbf{G} = [hk0]^*$, $h+k$ odd, Bragg reflection $\mathbf{G}$ always being stronger in intensity than the parallel lines on the low angle side—see Fig. 3a. Such an effect is observed regardless of exact tilt orientation. The similarity of the observed diffraction behaviour is indicative of the fact that the displacive shifts of the As ions responsible must clearly be very closely related for both ThAsSe and UAsSe [20,21].

That the $\mathbf{G} \pm \chi\langle 1\bar{1}0\rangle^* \pm \varepsilon\langle 110\rangle^*$ 'lines' of diffuse intensity characteristic of UAsSe shown in Fig. 3a are not in fact lines but rather part of an essentially continuous plane of diffuse intensity perpendicular to each of the two $\langle 110 \rangle$ real space directions, as is again also the case for ThAsSe, is confirmed by the $[11\bar{2}]$ zone axis EDP of UAsSe shown in Fig. 4. This EDP was obtained by tilting ~18.6° away from the [001] zone axis orientation of Fig. 3a around the $[1\bar{1}0]^*$ systematic row. Note that the transverse polarized diffuse streaking apparent in Fig. 3a is still present but this time runs along the $[1\bar{1}0]^*$ and [111]* reciprocal space directions around the hkl, $h+k$ odd, parent Bragg reflections. It remains present on tilting further around the $[1\bar{1}0]^*$ systematic row. The diffuse thus takes the form of continuous sheets of diffuse intensity perpendicular to the [110] and $[1\bar{1}0]$ directions respectively, again just as for ThAsSe (see [20]).

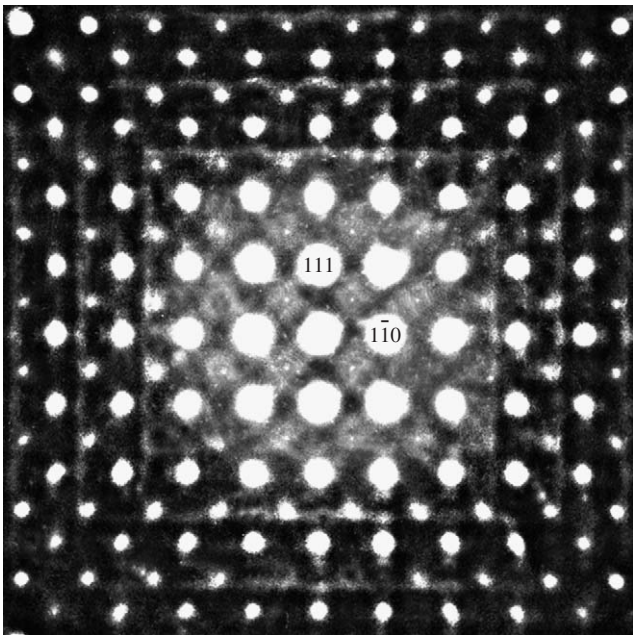

Fig. 4. A $[11\bar{2}]$ zone axis EDP of UAsSe again taken at ~80–90 K and obtained by tilting ~18.6 away from the [001] zone axis orientation of Fig. 3a around the $[1\bar{1}0]^*$ systematic row.

Again, as for ThAsSe, the polarized nature of the diffuse streaking apparent in Fig. 3a and 4 requires that the dominant contribution to the diffuse sheet perpendicular to [110] arises from atomic displacements along [110] in real space while the dominant contribution to the diffuse sheet perpendicular to $[1\bar{1}0]$ arises from atomic displacements along $[1\bar{1}0]$.

3. Pattern of As–As dimerization responsible

Following the same procedures as reported previously for ThAsSe [20], a plausible model for the pattern of atomic displacements responsible for the observed diffuse distribution in UAsSe (see Fig. 5) can be derived as follows: {110}* sheets of diffuse intensity in reciprocal space imply the existence of $\langle 110 \rangle$ rods of atoms in real space exhibiting displacements correlated along $\langle 110 \rangle$ but with essentially no correlation from one such rod to the next in the plane perpendicular to the rod direction. Thus the 1-d $\langle 110 \rangle$ As–As dimerization pattern in UAsSe associated with the observed $G \pm \sim 0.125\langle 110\rangle^* \pm \varepsilon\langle 1\bar{1}0\rangle^* \pm \eta[001]^*$ (ε and η essentially continuous) sheets of diffuse intensity arise from longitudinal $\langle 110 \rangle$ shifts of As ions along the $\langle 110 \rangle$ correlation direction associated with the 'primary modulation wave–vector', in this case $\mathbf{q} \sim 0.125\ \langle 110 \rangle^*$.

Formally there exist two distinct As sites per parent $P4/nmm$ unit cell: As1 at 000 and As2 at $\frac{1}{2}, \frac{1}{2}, 0$ (see Fig. 2). The fact that the $\mathbf{G} \pm \mathbf{q} \pm \varepsilon\langle 1\bar{1}0\rangle^* \pm \eta[001]^*$ diffuse streaking in Figs. 3a and 4 occurs only around the $\mathbf{G} = [hkl]^*$, $h+k$ odd, but not even, reflections can only arise from the interference between the displacement eigenvectors of these two C-centred related As ions (in this case a requirement that they move in the opposite direction). This can be seen from the relevant structure factor expression (see [21] for details)

$$F(\mathbf{G}+\mathbf{q}) = N\Sigma_\mu f_\mu \exp -2\pi i\mathbf{G}\cdot\mathbf{r}_\mu \times (2\pi[\mathbf{G}+\mathbf{q}]\cdot\mathbf{e}_\mu(\mathbf{q})) \times\left\{-\frac{i}{2}+\frac{i}{16}|2\pi[\mathbf{G}+\mathbf{q}]\cdot\mathbf{e}_\mu(\mathbf{q})|^2+\cdots\right\}. \quad (1)$$

In this functional form, and under the assumption that the shifts of the As ions make the largest contribution to $F(\mathbf{G}+\mathbf{q})$, it is easy to see why the $h+k$ odd, C-centred, pseudo-extinction condition occurs. All that is required is that $\mathbf{e}_{As2}$ (at $\mathbf{r}_{As2} = [\frac{1}{2},\frac{1}{2},0]$) must $= -\mathbf{e}_{As1}$ (at $\mathbf{r}_{As1} = [0,0,0]$) for $\mathbf{q} \sim 0.125\langle 110\rangle^*$ as substitution into the above expression shows. The most general possible displacive atomic modulation functions (AMFs, [22]) for these As ions compatible with the experimental observations is then

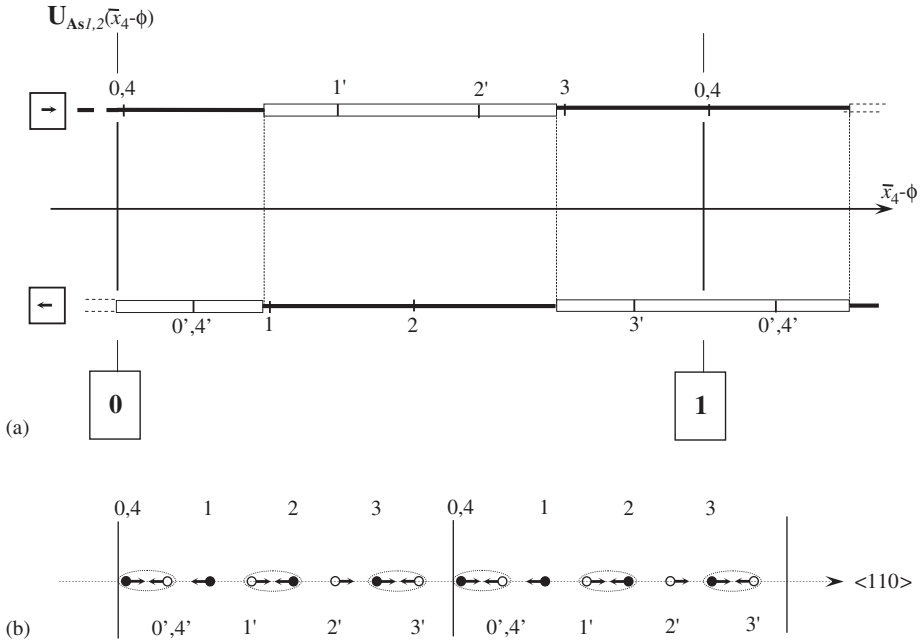

Fig. 5. (a) The square wave As1,2 displacive AMFs along the $(\bar{x}_4 - \phi)$ direction of super-space (the solid line represents the assumed displacive AMF of As1 while the 180° out of phase displacive AMF of As2 is represented by the open bar square wave). Note that $\bar{x}_4 = \mathbf{q}.[\mathbf{r}_{As1,2} + \mathbf{t}]$ where $\mathbf{q}\sim 0.125\ \langle 110\rangle^*$, $\mathbf{r}_{As1} = 0$, $\mathbf{r}_{As2} = \frac{1}{2}\langle 110\rangle$, $\mathbf{t} = \mathrm{m}\langle 110\rangle$, m an integer and ϕ is the global phase. The resultant predicted 1-d As–As dimerization pattern assuming $\phi = 0$ and $\mathbf{q} = \frac{1}{8}\langle 110\rangle^*$ exactly is shown in b.

given by

$$\mathbf{u}_{As1,2}(\bar{x}_4 = \mathbf{q}.[\mathbf{r}_{As1,2} + \mathbf{t}]) = \pm\varepsilon_{As}(\mathbf{a} + \mathbf{b}) \cos 2\pi(\bar{x}_4 - \phi) + \ldots \text{higher order harmonic terms}, \quad (2)$$

where the + sign refers to the As1 atoms, the − sign to the As2 atoms, $\mathbf{q}\sim 0.125\ \langle 110\rangle^*$ and ϕ represents the so-called global phase [22]. For the purposes of deriving a plausible As–As dimerization pattern, we have assumed an inherently square wave shape for the above displacive AMF (see Fig. 5a) i.e. for $-\frac{1}{4} < (\bar{x}_4 - \phi) < \frac{1}{4}$ along the $(\bar{x}_4 - \phi)$ direction of hyper-space we ascribe a value of +1 to $\cos 2\pi(\bar{x}_4 - \phi)$ in Eq. (1) above and for $+\frac{1}{4} < (\bar{x}_4 - \phi) < \frac{3}{4}$ we ascribe a value of −1. The resultant predicted As–As dimerization pattern assuming $\phi = 0$ and $\mathbf{q} = \frac{1}{8}\langle 110\rangle^*$ exactly is shown in Fig. 5b.

As for ThAsSe [20], it seems that the structural origin of the low temperature Kondo effect in UAsSe can again be ascribed to the gradual condensation of a CDW associated with As–As dimerization. The question of why the periodicity associated with this As–As dimerization along the $\langle 110\rangle$ directions has the periodicity it does, however, remains. To attempt to find an answer to this question we now turn to Extended Hückel tight binding calculations of the electronic band structures of both ThAsSe and UAsSe.

4. Band structure calculations

In order to gain insight into the FS nesting presumed responsible for the diffraction phenomena observed above, in particular for the observed magnitude of χ, electronic band structure calculations within the extended Hückel tight binding (EHTB) approximation [23–25] have been performed. In this approach, tight-binding Hamiltonians are defined as one-electron operators for the valence electrons only, thus neglecting core effects and electron–electron repulsion. The valence orbitals are approximated by Slater-type orbitals taken from first-principle calculations for the pure elements. The diagonal elements of the Hamiltonian are defined as the valence state ionization potentials (VSIP): $H_{\mu\mu} = -(\text{VSIP})$, whilst the off-diagonal elements are defined semi-empirically by the Wolfsberg-Helmholz formula: $H_{\mu\upsilon} = KS_{\mu\upsilon}\ (H_{\mu\mu} + H_{\upsilon\upsilon})/2$, where $S_{\mu\upsilon}$ is the overlap matrix between the two states χ_μ and χ_υ and K is a constant. The method thus uses input parameters from first-principles calculations defining the atomic orbitals and allows the Hamiltonian of the system to be solved non-self-consistently.

The method has been used very successfully to describe the electronic properties of a wide range of periodic and non-periodic systems [26,27], as well as CDW phenomena in transition-metal chalcogenide systems (see e.g. [28]). In the present work the CAESAR package [25] was applied to calculate dispersion curves (DCs), (partial) density of states (P)(DOSs) and FSs for both ThAsSe and UAsSe. The goal was to look for possible CDW nesting conditions, which could then be compared with the experimentally obtained **q**-vectors i.e. with the magnitude of χ. The effects of As–As dimerization on the DOS spectra as well as of interchanging As and Se positions in the unit cell were also examined. No details of any band structure calculations on these compounds have previously been reported, although

a band structure calculation within the local-spin-density approximation (LSDA) has been performed on UAsSe and used to calculate its magneto-optical Kerr spectra [29].

Initially, the electronic properties of the undistorted ThAsSe and UAsSe average structures were calculated, using the reported $P4/nmm$ average structures and lattice parameters ($a = 4.084$, $c = 8.578$ Å for ThAsSe and $a = 3.987$, $c = 8.381$ Å for UAsSe). The extended Hückel potential parameters used in the calculations are given in Table 1. Electronic properties were calculated by sampling 1331 points from the irreducible region of **k**-space. The calculated DCs of undistorted (a) ThAsSe and (b) UAsSe are shown in Figs. 6a and b. (In the case of ThAsSe, the relative contributions of the Th 5*f* and As 4*p* orbitals to the three bands nearest to the Fermi level, E_f, are shown in Fig. 6c). The corresponding (P)DOS spectra are shown in Figs. 7a and b while the calculated FSs are shown along a close to [001] projection in Figs. 8a and b.

Note that the DOS at the Fermi level (E_f) is significantly larger in the case of UAsSe than in the case of ThAsSe and that the dominant contribution to the DOS comes from U *f*-orbitals (cf. Fig. 7b with a). (The previous band structure calculation of UAsSe also reported significant *f*-band character in the vicinity of the FS [29]). In the case of ThAsSe, note that while the contribution to the DOS at the Fermi level (E_f) from Th 5*f*-orbitals is significantly reduced, it still remains the major contributor i.e. Th 5*f*-orbitals are at least partially populated at E_f.

Interestingly, however, Fig. 6c shows that there is nonetheless significant admixture of As 4*p* orbitals with Th 5*f* orbitals in specific wave-vector regions in the two bands which cross the Fermi level and that the amount of this admixture seems to be directly related to the dispersion of these bands and hence to the shape of the FS itself. Where the admixture of As 4*p* orbitals is absent, e.g.

Table 1
Extended Hückel parameters from the CEASAR package used in the electronic band structure calculations [25]

	Exponents			
Orbital		H_{ii} (eV)	1a	2a
Th	7*s*		−5.39	1.834
	7*p*		−5.39	1.834
	6*d*	−10.11	2.461 (0.7612)	1.165(0.4071)
	5*f*	−9.64	4.477(0.7682)	1.837(0.4267)
U	7*s*	−5.5	1.914	
	7*p*	−5.5	1.914	
	6*d*	−9.19	2.581(0.7608)	1.207(0.4126)
	5*f*	−10.62	4.943(0.7844)	2.106(0.3908)
As	4*s*	−16.219999	2.23	
	4*p*	−12.16	1.89	
Se	4*s*	−20.5	2.44	
	4*p*	−13.2	2.07	

'a' Exponents and coefficients (in parentheses) in a double-expansion of the metal *d* orbitals.

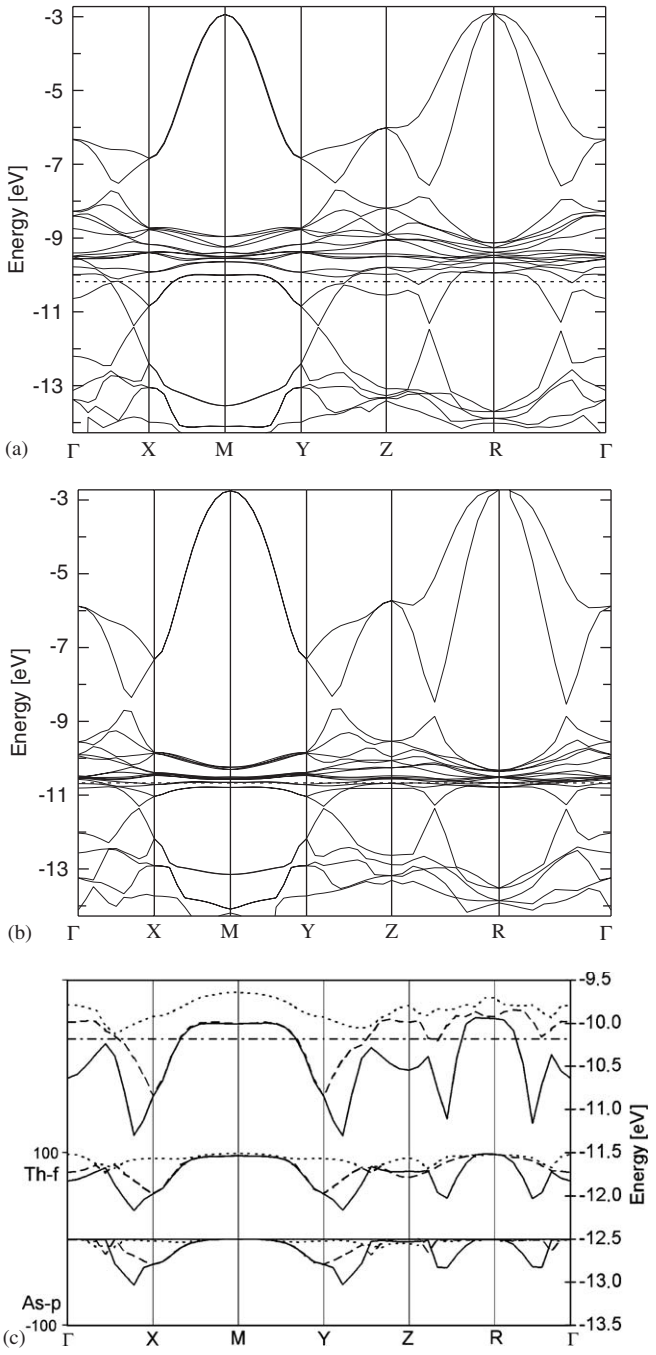

Fig. 6. The calculated dispersion curves (DCs) of the undistorted average or parent ($a_p \times a_p \times c_p$) structures of (a) ThAsSe and (b) UAsSe. The Fermi level, E_f, is marked by the dashed horizontal line in both cases. In (c) the relative contributions of the Th 5*f* and As 4*p* orbitals to the three bands (No. 15 ——, No. 16 - - - and No. 17 ….) closest to the Fermi level (marked by the horizontal -.-.- line) are shown for non-modulated ThAsSe. The top part of the figure is essentially a blow-up of Fig. 6a in the vicinity of the Fermi level, E_f. In the bottom part of the figure, the Th 5*f* contribution at each wave-vector is shown above the solid zero line in the range from 0 to 100 while the corresponding As 4*p* contribution at the same wave-vector is shown below the solid zero line (in the range 0 to −100). Note that the energy of bands 15 and 16 drop significantly whenever there is significant admixture of the Th 5*f* and As 4*p* orbitals.

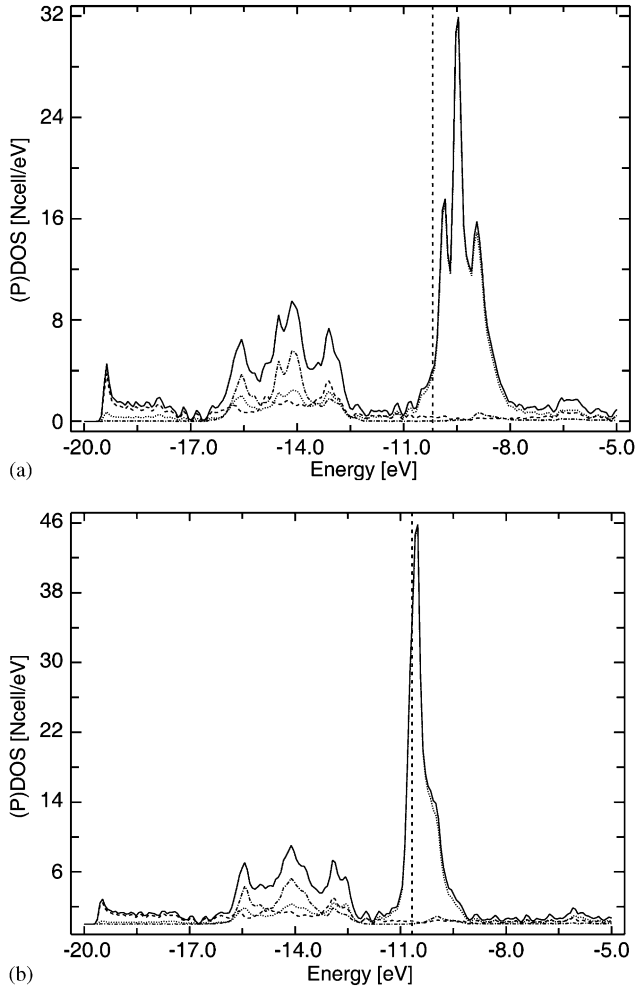

Fig. 7. Partial density of states (PDOS) curves (solid line = total DOS, …. line = the Th contribution, - - - = the As contribution and -. - .-. = the Se contribution) corresponding to the undistorted average ($a_p \times a_p \times c_p$) structures of (a) ThAsSe and (b) UAsSe. E_f is marked by the dashed vertical line in both cases. Note that the DOS at E_f is nearly entirely determined by Th and U *f*-electrons, respectively.

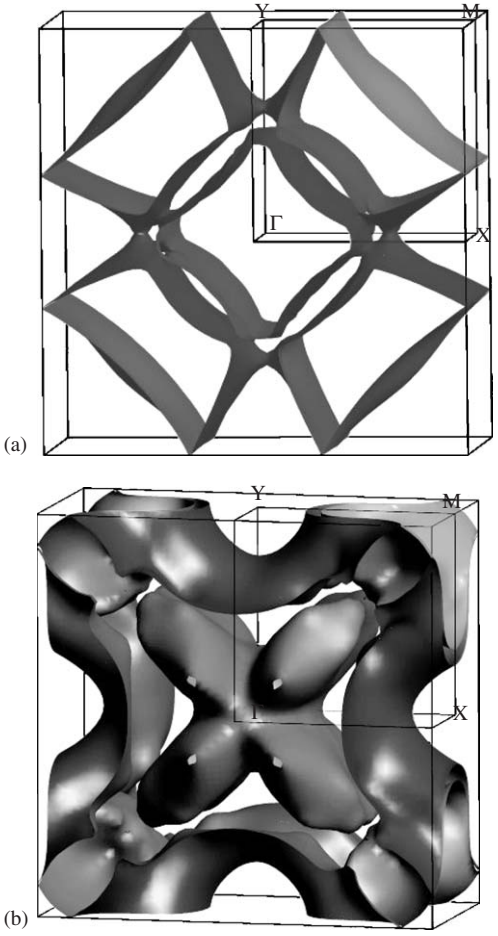

Fig. 8. FSs of the basic ($a_p \times a_p \times c_p$) structures of (a) ThAsSe and (b) UAsSe projected close to the [001]* direction. The first Brillouin zone is shown outlined in both cases while the Γ (**0**), $X(\frac{1}{2}\mathbf{a}*)$, $Y(\frac{1}{2}\mathbf{b}*)$ and $M(\frac{1}{2}\mathbf{a}* + \frac{1}{2}\mathbf{b}*)$ points of reciprocal space are also marked.

around the M or R points (see Fig. 6c), the corresponding bands are very flat (see Fig. 6a). On moving away from the *M* point towards the *X*, *Y* points or from the *R* towards the *Z* point, however, significant admixture with As 4*p* orbitals occurs and the bands drop suddenly in energy leading to their crossing the Fermi level and hence determining the FS shape in Fig. 8a.

To check whether this sudden drop in energy is a direct result of an admixture between the Th 5*f* and the As 4*p* states, crystal orbital overlap population (COOP) diagrams were calculated for non-modulated ThAsSe and compared with the corresponding PDOS diagrams of non-modulated ThAsSe. The COOP diagram, which divides the PDOS into bonding and antibonding segments, shows that only the Th–As overlap has a bonding character at E_f. All other overlaps either have an antibonding character (As–As) or can be neglected at E_f, including direct Th–Th overlap. This suggests that the *f* electrons in the Th layers do not move directly from Th to Th but rather via the As layers and back again. The overlapped Th–As bonding orbitals thus seem to be important for basal plane conductivity.

The calculated FSs of (a) ThAsSe and (b) UAsSe are shown along a close to [001] projection in Fig. 8. Note that both FSs, in particular that of ThAsSe, are markedly quasi two-dimensional in character and that appropriate nesting vectors are thus indeed likely to take the desired $\chi\langle 110\rangle^* \pm \varepsilon\langle 1\bar{1}0\rangle^* \pm \eta[001]^*$ (χ fixed, ε, η continuous) form. Projections of both FSs onto the basal plane perpendicular to c^* are shown in Fig. 9. Potential modulation vectors, which span parallel sections of the FSs and obviously support nesting, are indicated by the arrows in Fig. 9. The magnitudes of these nesting wave-vectors along the $\langle 110\rangle^*$ directions (0.14 $\langle 110\rangle^*$ and 0.12 $\langle 110\rangle^*$, respectively) are in rather good accord with the experimental values for χ determined from the experimentally observed diffuse distributions given above. Thus the periodicities of the As–As dimerization apparent in the observed diffuse distributions (see Fig. 3) appear to be directly related to the FSs of both ThAsSe and UAsSe.

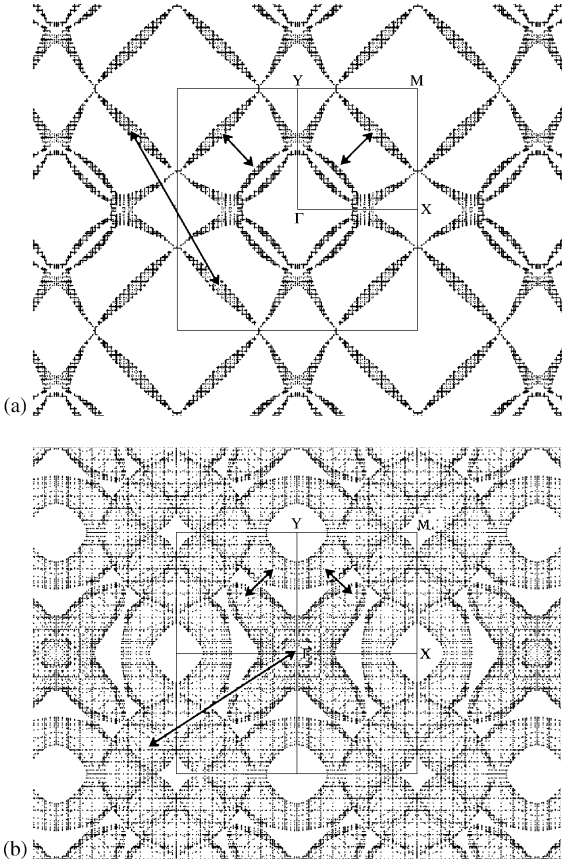

Fig. 9. FS projections along the $\boldsymbol{c}^*$ direction of the undistorted average ($a_p \times a_p \times c_p$) structures of (a) ThAsSe and (b) UAsSe. Modulation **q**-vectors, determined experimentally from the electron diffraction experiments are indicated. The square first Brillouin zone is outlined and the Γ (**0**), $X(\frac{1}{2}\mathbf{a}*)$, $Y(\frac{1}{2}\mathbf{b}*)$ and $M(\frac{1}{2}\mathbf{a}* + \frac{1}{2}\mathbf{b}*)$ points of reciprocal space marked.

As a result of the extensive prominence given in the literature to the effect of possible As/Se disorder upon the electrical transport properties of UAsSe [12–18], calculations with interchanged As/Se positions were also performed. Three distinct variants with interchanged As and Se positions were considered. All, however, gave similar results and very similar calculated Fermi surfaces (FSs), supporting the conclusion that the electrons in the vicinity of E_f are indeed predominantly coming from Th (or U) *f*-orbitals.

In addition to the above calculations performed on the undistorted ($a_p \times a_p \times c_p$, subscript p for parent) average or parent structures, an attempt was also made to investigate the effect of As–As dimerization on the electronic band structure in the vicinity of the FS using a ($7a_p \times 7a_p \times c_p$) superstructure model for ThAsSe described in [20]. Keep in mind, however, that this is only a model meant to give an idea of the As shifts occurring in the As layers and not an accurate reflection of what is actually occurring. Due to the massively enlarged basal plane unit cell, the FSs are multiply folded in **k**-space making it difficult to directly compare DCs etc. with those of the undistorted structure. The effect of As–As dimerization was thus followed only in

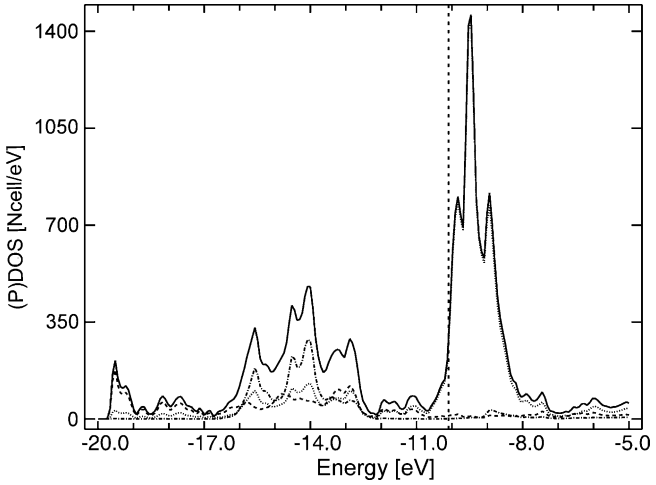

Fig. 10. PDOS curves (solid line = total DOS, ... line = the Th contribution, - - - = the As contribution and -.-.-. = the Se contribution) calculated using a modulated ($7a_p \times 7a_p \times c_p$) superstructure model of ThAsSe derived from Withers et al. [20].

the corresponding (P)DOS spectra. Surprisingly little change, however, could be observed in the (P)DOS spectra (cf. Fig. 10 with Fig. 7a). The main contribution to the PDOS in the vicinity of E_f remained that from the Th *f*-orbitals and no obvious signs of a band gap were apparent.

5. Conclusions

The temperature-dependent electron diffraction results confirm that the highly structured diffuse intensity distributions characteristic of the low temperature reciprocal spaces of both ThAsSe and UAsSe are the result of the gradual condensation of a CDW associated with As–As dimerization along ⟨110⟩ real space directions. The electronic band structure calculations show that the (in general) incommensurate periodicity of this As–As dimerization along the two ⟨110⟩ real space directions is determined by the FS of the undistorted parent structures, despite the fact that the electrons in the vicinity of E_f predominantly come from Th (or U) *f*-orbitals. These calculations also show that partial As/Se occupational disorder has no major influence either on the shape of the resulting FSs or on the distances between the parallel sections responsible for nesting.

The **q**-vectors, obtained by measuring the distances between the flattened parts of the corresponding FSs are in remarkably good accord with the values determined from the TEM experiments. The presence of a large (multiple) peak in the (P)DOS curves in the vicinity of E_f which undoubtedly belongs to Th/U and not As (see Fig. 7) is an intriguing result given that the major contribution to the intensity of the observed diffuse distribution is clearly due to As–As dimerization. The overall instability may be triggered in the low-dimensional electron gas and then be followed by the As–As dimerization, or vice-versa i.e. the

As–As dimerization may stabilize the the modulated ground state by lowering the electronic energy of the occupied states in the vicinity of the FS. Further progress as to the mechanism for overall energy lowering, however, probably requires more detailed and higher level band structure calculations beyond the scope of the current contribution.

Acknowledgments

RLW acknowledges the Ausralian Research Council (ARC) for financial support in the form of an ARC Discovery Grant. AP and HJPvM thank the Ministry of Science and Higher Education of the Republic of Slovenia for a research grant.

References

[1] F. Hulliger, J. Less-Common Metals 16 (1968) 113–117.
[2] A. Wojakowski, Z. Henkie, Z. Kletowski, Phys. Stat. Solidi (a) 14 (1972) 517–520.
[3] J. Schoenes, W. Basca, F. Hulliger, Solid State Commun. 68 (1988) 287–289.
[4] J. Kondo, Prog. Theor. Phys. Osaka 32 (1964) 37–47.
[5] J. Leciejewicz, A. Zygmunt, Phys. Stat. Solidi (a) 13 (1972) 657–660.
[6] A. Wojakowski, Z. Henkie, Acta Phys. Pol. A 52 (1977) 401–411.
[7] J. Brunner, M. Erbudak, F. Hulliger, Solid State Commun. 38 (1981) 841–843.
[8] W. Reim, J. Schoenes, F. Hulliger, Physica B 130 (1985) 64–65.
[9] Z. Henkie, R. Fabrowski, A. Wojakowski, J. Alloys Compounds 219 (1995) 248–251.
[10] D.L. Cox, A. Zawadowski, Adv. Phys. 47 (1998) 599–642.
[11] Z. Henkie, A. Pietraszko, A. Wojakowski, L. Kepinski, T. Cichorek, J. Alloys Compounds 317-318 (2001) 52–59.
[12] Z. Henkie, T. Cichorek, A. Pietraszko, R. Fabrowski, A. Wojakowski, B.S. Kuzhel, L. Kepinski, L. Krajczyk, A. Gukasov, P. Wisniewski, J. Phys. Chem. Solids 59 (1998) 385–393.
[13] Z. Henkie, T. Cichorek, R. Fabrowski, A. Wojakowski, B.S. Kuzhel, Cz. Marucha, M.S. Szczepaniak, J. Tadla, Physica B 281-282 (2000) 226–227.
[14] T. Cichorek, Z. Henkie, P. Gegenwart, M. Lang, A. Wojakowski, M. Dischner, F. Steglich, J. Magn. Magn. Mater. 226-230 (2001) 189–190.
[15] T. Cichorek, Z. Henkie, A. Wojakowski, A. Pietrasko, P. Gegenwart, M. Lang, F. Steglich, Solid State Commun. 121 (2002) 647–651.
[16] T. Cichorek, R. Wawryk, A. Wojakowski, Z. Henkie, F. Steglich, Acta Phys. Polonica 34 (2003) 1339–1344.
[17] T. Cichorek, H. Aoki, J. Custers, P. Gegenwart, F. Steglich, Z. Henkie, E.D. Bauer, M.B. Maple, Phys. Rev. B 68 (2003) 144411:1–7.
[18] T. Cichorek, A. Sanchez, P. Gegenwart, F. Weickert, A. Wojakowski, Z. Henkie, G. Auffermann, S. Paschen, R. Kniep, F. Steglich, Phys. Rev. Letts. 94 (2005) 236603:1–4.
[19] F. Hulliger, P 258, in: F. Lévy (Ed.), Structural Chemistry of Layer-Type Phases, D. Reidel, Dordrecht, 1976.
[20] R.L. Withers, R. Vincent, J. Schoenes, J. Solid State Chem. 177 (2004) 701-108.
[21] R.L. Withers, Z. für Kristallogr. 220 (2005) 1027–1034.
[22] R.L. Withers, S. Schmid, J.G. Thompson, Prog. Solid State Chem. 26 (1998) 1–96.
[23] M.-H. Whangbo, R. Hoffmann, J. Am. Chem. Soc. 100 (1978) 6093–6098.
[24] M.-H. Whangbo, R. Hoffmann, R.B. Woodward, Proc. Roy. Soc. Lond. Ser. A 366 (1979) 23–36.
[25] J. Ren, W. Liang, M.-H. Whangbo, CEASAR program, PrimeColour Software Inc., Cary, NC, 1998.
[26] (a) T.R. Ward, R. Hoffmann, M. Shelef, Surf. Sci. 289 (1993) 85–99;
(b) D.L. Vuckovic, S.A. Jansen, R. Hoffmann, Langmuir 6 (1990) 732–746;
(c) M.C. Zonnevylle, R. Hoffmann, Langmuir 3 (1987) 452–459.
[27] (a) Z.X. Yang, K. Zhang, X. Xie, Surf. Sci. 382 (1997) 100–106;
(b) H. Fu, L. Ye, K. Zhang, X. Xie, Surf. Sci. 341 (1995) 273–281;
(c) I. Efremenko, M. Sheintuch, Surf. Sci. 414 (1998) 148–158;
(d) P. Sonnet, L. Stauffer, S. Saintenoy, C. Piffi, P. Wetzel, G. Gewinner, C. Minot, Phys. Rev. B 56 (1997) 15171–15179;
(e) C. Noce, M. Cuoco, Phys. Rev. B 59 (1999) 2659–2666.
[28] E. Canadell, M.H. Whangbo, Inorg. Chem. 25 (1985) 1488–1491.
[29] P.M. Oppeneer, M.S.S. Brooks, V.N. Antonov, T. Kraft, H. Eschrig, Phys.Rev.B 53 (1996) R10437–R10440.